n-CdSe/*p*-ZnTe based wide band-gap light emitters: Numerical simulation and design

M. W. Wang, M. C. Phillips, J. F. Swenberg, E. T. Yu,[a] J. O. McCaldin, and T. C. McGill
T. J. Watson, Sr., Laboratory of Applied Physics, California Institute of Technology, Pasadena, California 91125

(Received 13 August 1992; accepted for publication 4 January 1993)

The only II-VI/II-VI wide band-gap heterojunction to provide both good lattice match and *p*- and *n*-type dopability is CdSe/ZnTe. We have carried out numerical simulations of several light emitter designs incorporating CdSe, ZnTe, and Mg alloys. In the simulations, Poisson's equation is solved in conjunction with the hole and electron current and continuity equations. Radiative and nonradiative recombination in bulk material and at interfaces are included in the model. Simulation results show that an *n*-CdSe/*p*-ZnTe heterostructure is unfavorable for efficient wide band-gap light emission due to recombination in the CdSe and at the CdSe/ZnTe interface. An *n*-CdSe/$Mg_xCd_{1-x}Se$/*p*-ZnTe heterostructure significantly reduces interfacial recombination and facilitates electron injection into the *p*-ZnTe layer. The addition of a $Mg_yZn_{1-y}Te$ electron confining layer further improves the efficiency of light emission. Finally, an *n*-CdSe/$Mg_xCd_{1-x}Se$/$Mg_yZn_{1-y}Te$/*p*-ZnTe design allows tunability of the wavelength of light emission from green into the blue wavelength regime.

I. INTRODUCTION

A fundamental problem in fabricating wide gap binary II-VI light-emitting diodes (LEDs) has been the inability to obtain both *n*- and *p*-type doping in these materials by conventional doping techniques. Recently, this limitation has been partially overcome by nitrogen plasma doping to produce *p*-ZnSe with hole concentrations up to 10^{18} cm^{-3}.[1] Although such doping has led to the demonstration of the first blue-green laser diodes,[2] hole concentrations are still not high enough to afford ohmic contacts to *p*-ZnSe. Thus, the realization of highly doped *p*-ZnSe is still a major obstacle to the further development of ZnSe based LEDs and laser diodes. An alternative solution to the dopability problem is to use a heterojunction formed between a naturally *n*-type and a naturally *p*-type material.

In this paper, we examine the simulation and design of II-VI heterostructure LEDs based on *n*-CdSe and *p*-ZnTe. We choose these two semiconductors because of their favorable dopability and close lattice match. The drift-diffusion model, modified to account for heterojunctions, is used in our simulations. To determine LED design feasibility, bulk and interfacial recombination are included in the model. Details of the model are given in Sec. II. Some of the more important parameters accounted for in the design process are band offsets, lattice mismatch, dopability, and interfacial effects. Where unknown, band offsets used in the simulations are estimated using the common anion rule.[3] We emphasize here that the simulation results are not dependent on the validity of this rule, as demonstrated in one simulation in which an undesirable deviation from the common anion rule is used. Details of the design methodology are discussed in Sec. III. Simulation results are presented in Sec. IV. A simple CdSe/ZnTe heterojunction is first presented, followed by a CdSe/$Mg_xCd_{1-x}Se$/ZnTe heterostructure design utilizing a graded injector to facilitate electron injection.[4] Next, a design incorporating a $Mg_xZn_{1-x}Te$ electron confining layer is presented. Finally, a device design that allows tunability of the wavelength of light emission from green to blue is proposed and analyzed. Section V concludes the paper.

II. MODEL

In our simulations, we use the drift-diffusion transport equations to solve for the CBE and VBE, as well as the charge and current densities. For a homostructure, the basic equations to be solved in the drift-diffusion model are Poisson's equation, the electron and hole current equations, and the electron and hole continuity equations. In one dimension, assuming steady-state conditions and spatially constant temperatures, these equations are

$$\frac{dE}{dx}=\frac{e}{\epsilon}(p-n+N_d^+-N_a^-), \tag{1}$$

$$j_p=e\mu_p pE-eD_p\frac{dp}{dx}, \tag{2}$$

$$j_n=e\mu_n nE+eD_n\frac{dn}{dx}, \tag{3}$$

$$\frac{dj_p}{dx}=-eU-eB(pn-n_i^2), \tag{4}$$

$$\frac{dj_n}{dx}=eU+eB(pn-n_i^2), \tag{5}$$

where E is the electric field, n and p are the electron and hole concentrations, and ϵ is the dielectric constant. D, μ, and j refer to the diffusion constant, mobility, and current

[a]Now at Department of Electrical and Computer Engineering, University of California, San Diego, La Jolla, CA 92093.

 0021-8979/93/094660-09$06.00

density, respectively, where the subscripts p and n refer to holes and electrons, respectively. B is the probability for radiative recombination, and U is the indirect recombination rate, described in detail below. N_d^+ and N_a^- are the concentrations of ionized donors and acceptors given by

$$N_d^+=\frac{N_d}{1+2\exp[(E_{fn}-E_d)/k_bT]}, \tag{6}$$

$$N_a^-=\frac{N_a}{1+4\exp[(E_a-E_{fp})/k_bT]}, \tag{7}$$

where E_{fn} and E_{fp} are the electron and hole quasi-Fermi levels, respectively. The electron and hole quasi-Fermi levels are determined from the carrier concentrations using standard Fermi-Dirac statistics.

The van Roosbroeck–Shockley method of equating equilibrium band-to-band recombination and absorption rates[5] is used to estimate B. The optical absorption coefficient required for this calculation is determined as detailed in Ref. 6. The final expression for the radiative recombination rate is

$$B=\left(\frac{2\pi}{k_bTc^2(m_e+m_h)}\right)^{3/2}\frac{\hbar e^2 n_r}{12\pi\epsilon_0}\left(\frac{1}{m}+\frac{1}{m_e}+\frac{1}{m_h}\right)E_g^2, \tag{8}$$

where n_r is the index of refraction, E_g is the band gap of the semiconductor, ϵ_0 is the permittivity of free space, and c is the speed of light in vacuum.

The indirect recombination rate U for a single trapping level is given by standard Shockley–Read–Hall statistics[7]

$$U=\frac{np-n_i^2}{(p+p_1)\tau_n+(n+n_1)\tau_p}, \tag{9}$$

where τ_n and τ_p are the electron and hole lifetimes, and n_1 and p_1 are given by

$$n_1=N_c\exp[(E_t-E_c)/k_bT], \tag{10}$$

$$p_1=N_v\exp[(E_v-E_t)/k_bT]. \tag{11}$$

N_c and N_v are the effective densities of states for electrons and holes, respectively, and E_t is the energy of the trap level.

To model heterostructures, Eqs. (1)–(5) must be modified slightly.[8,9] The modified equations are as follows:

$$\frac{dE}{dx}=\frac{e}{\epsilon}(N_d^+-N_a^--n+p)-\frac{E}{\epsilon}\frac{d\epsilon}{dx}, \tag{12}$$

$$j_p=e\mu_p pE-\mu_p p\frac{d(\chi+E_g)}{dx}-eD_p\frac{dp}{dx}+\frac{eD_p p}{N_v}\frac{dN_v}{dx}, \tag{13}$$

$$j_n=e\mu_n nE-\mu_n n\frac{d\chi}{dx}+eD_n\frac{dn}{dx}-\frac{eD_n n}{N_c}\frac{dN_c}{dx}, \tag{14}$$

$$\frac{dj_p}{dx}=-eU_b-eU_i-eB(pn-n_i^2), \tag{15}$$

$$\frac{dj_n}{dx}=eU_b+eU_i+eB(pn-n_i^2), \tag{16}$$

where χ and E_g are the electron affinity and band gap of the semiconductor. U_b and U_i refer to the bulk and interfacial recombination rates.

The physical interpretation of the additional heterostructure terms in Eqs. (12)–(16) is given below. More detailed derivations and discussions of the above heterostructure drift-diffusion equations can be found in Refs. 8 and 10. The last term in Eq. (12) simply imposes continuity of displacement at the interface between two different materials. The second term on the right-hand side of Eqs. (13) and (14) is a drift component due to what is labeled a quasi-electric field for holes or electrons.[10,11] The hole quasi-electric field,

$$\frac{1}{e}\frac{d(\chi+E_g)}{dx}, \tag{17}$$

is an additional field influencing holes in graded regions and at interfaces, where the valence band has an additional slope due to valence-band offsets (VBO) between the materials in question. Similarly, electrons feel a quasi-electric field,

$$\frac{1}{e}\frac{d\chi}{dx}, \tag{18}$$

due to conduction-band offsets (CBO). Known or estimated band offsets are used to determine the positional variation of the electron affinity. The last term of Eq. (13) is a diffusion-like term resulting from a position-dependent effective density of states (DOS). This term causes holes to diffuse from regions of low DOS to regions of high DOS. A similar term appears in Eq. (13) for electrons. The bulk recombination U_b is given by Eq. (9). Finally, an additional interfacial recombination term has been added to Eqs. (15) and (16), since interfacial recombination can have a significant effect on heterostructure device operation. The interfacial recombination due to trap levels produced by dangling bonds was implemented using a modified Shockley–Read–Hall model,[9,12] as given below:

$$U_i=\frac{(np-n_i^2)}{t(p+p_1)/S_n+t(n+n_1)/S_p}, \tag{19}$$

where

$$S_n=v_{\rm th}\sigma_n N_{st}, \tag{20}$$

$$S_p=v_{\rm th}\sigma_p N_{st}, \tag{21}$$

$$N_{st}=\frac{4(a_2^2-a_1^2)}{a_1^2a_2^2}. \tag{22}$$

In Eqs. (19)–(22), S_n and S_p are the surface recombination velocities for electrons and holes, respectively, $v_{\rm th}$ is the thermal velocity, N_{st} is the trap density per unit area, σ_n and σ_p are the capture cross sections for holes and electrons, respectively, a_1 and a_2 are the lattice parameters of the two semiconductors comprising the interface, and t is the thickness of the interface between the two semiconductors. Note that Eq. (19) assumes a single trap level at midgap, and Eq. (22) assumes that the growth is in the [100] direction, and that all of the lattice mismatch be-

tween the two semiconductors comprising an interface is taken up by dislocations and not by strain. In regions where part of the lattice mismatch is taken up by strain, Eq. (22) gives the upper limit for N_{st}.

In regions of varying composition, x, the dielectric constant and effective mass are given by[13]

$$\frac{\epsilon-1}{\epsilon+2}=x\left(\frac{\epsilon_1-1}{\epsilon_1+2}\right)+(1-x)\left(\frac{\epsilon_2-1}{\epsilon_2+2}\right), \tag{23}$$

$$\frac{1}{m^*}=\frac{x}{m_1^*}+\frac{1-x}{m_2^*}, \tag{24}$$

where x is the mole fraction of material 1. The band gap in graded regions can be modeled by[14]

$$E_g=A+Bx+Cx^2, \tag{25}$$

where A is the band gap for material 1 and B and C are experimentally determined parameters. The devices that we are modeling have graded regions where Eq. (25) is applicable; however, values for B and C are not known for the materials in certain regions. In these regions, we have assumed a linear dependence of E_g on material composition. Also, we have neglected the effects of strain on band structure in lattice-mismatched graded regions.

In heterostructures, regions with high electric fields and carrier concentrations are common, so the assumption of a constant mobility and the use of the nondegenerate form of Einstein's equation is no longer valid. The mobility as a function of both the field strength and the doping concentration is given by[15,16]

$$\mu_{n,p}^*=\mu_{n0,p0}+\mu_{n1,p1}\left[1+\left(\frac{N_d+N_a}{N_{n,p}}\right)^{\alpha_{n,p}}\right]^{-1}, \tag{26}$$

$$\mu_n=\left[\mu_n^*+\frac{V_{\rm sat}}{E}\left(\frac{E}{E_0}\right)^4\right]\left[1+\left(\frac{E}{E_0}\right)^4\right]^{-1}, \tag{27}$$

$$\mu_p=\mu_p^*\left[1+\frac{\mu_p^* E}{v_m}\right]^{-1}, \tag{28}$$

where E is the electric field, N_d and N_a refer to donor and acceptor concentrations, respectively, and subscripts n and p refer to electrons and holes, respectively. N, α, E_0, $V_{\rm sat}$, and v_m are experimentally determined parameters. These parameters are not generally known for the materials used in our devices, so as an initial approximation, we have used N, α, and E_0 as determined for GaAs. μ_0 and μ_1 are determined by using the same ratio of μ_0 to μ_1 as for GaAs, while constraining μ^* equal to experimental values of mobility in our materials for zero field and low-doping concentrations. The high-field saturation velocities $V_{\rm sat}$ and v_m, are set to one-half the peak velocities estimated from E_0 and μ^*. While not ideal, the method outlined above will give, to first order, trends in the change in mobility with respect to variations in field strength and doping concentration. It is necessary to include field dependent mobilities in the model, because in regions with high fields the ratio of diffusivity to mobility becomes large. If the decrease in mobility with increasing field is not accounted for, unrealistically large diffusion constants will result.

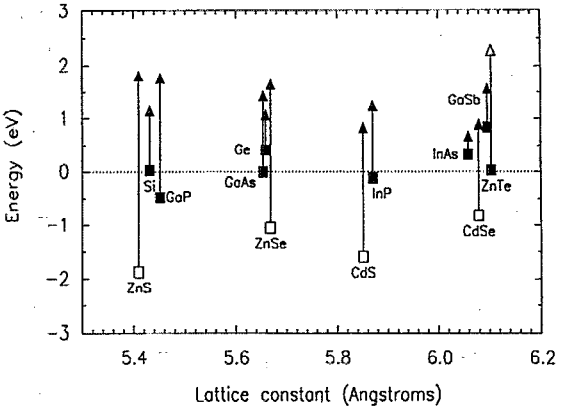

FIG. 1. McCaldin diagram for common semiconductors. Each material is represented by a vertical line with a square at the bottom, corresponding to the VBE, and a triangle at the top, corresponding to the CBE. The horizontal position of each line is determined by the lattice parameter. The length of each line scales with the band gap of the material that it represents. The vertical position of each line is determined by the respective VBO calculated using Harrison's LCAO method. Open triangles and squares represent semiconductors that cannot be doped n or p type, respectively, using conventional doping techniques. The zero of energy is chosen to be the VBE of GaAs.

As mentioned above, in regions of high carrier concentrations, the ratio of diffusivity to mobility can deviate significantly from k_bT/e. If the original derivation of the drift-diffusion equations from Boltzmann's equation is done without assuming Boltzmann statistics, then the following general form of Einstein's relation is obtained:[10]

$$\frac{D}{\mu}=\frac{2k_bTF_{1/2}(\eta)}{eF_{-1/2}(\eta)}, \tag{29}$$

where F_j is the Fermi-Dirac integral of order j, and η is $(E_{fn}-E_c)/k_bT$ for electrons, and $(E_v-E_{fp})/k_bT$ for holes. Analytic expressions approximating $F_{1/2}$ and $F_{-1/2}$ (Ref. 17) were used to evaluate Eq. (29).

The numerical solution of Eqs. (12)–(16) was carried out using the relaxation method.[18] Successful implementation of this method relies on reasonable choices of scaling factors and initial guesses.[19] Initial guesses were determined as in Ref. 20. Variable mesh spacing was incorporated, with larger mesh densities used in regions of rapid potential variation. Finally, abrupt junctions were graded over a distance of a few angstroms to avoid numerical instabilities that are introduced by singularities at an abrupt interface. The simulation results do not depend on the grading distances of the interfaces as long as they are not unreasonably large. For example, shortening the grading distance of an interface causes only the individual derivative terms in Eq. (13) to increase in magnitude, with no net effect on the overall current density.

III. DESIGN METHODOLOGY

In the design of heterostructure devices, it is often useful to first examine a diagram which simultaneously exhibits its lattice parameters, band offsets, and dopability for the materials of interest. We show such a diagram in Fig. 1,

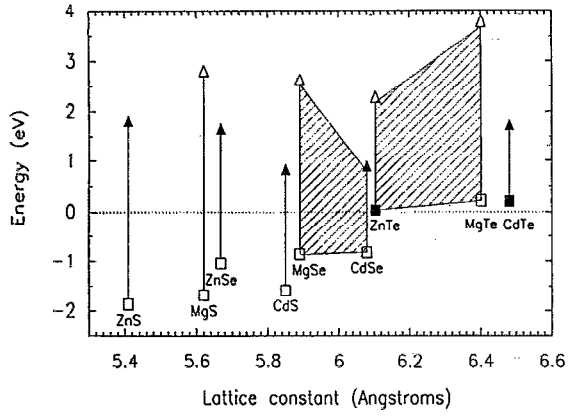

FIG. 2. McCaldin diagram for some commonly used II-VI materials with the addition of MgSe and MgTe. $Mg_xCd_{1-x}Se$ and $Mg_xZn_{1-x}Te$ ternaries are represented by the two shaded regions.

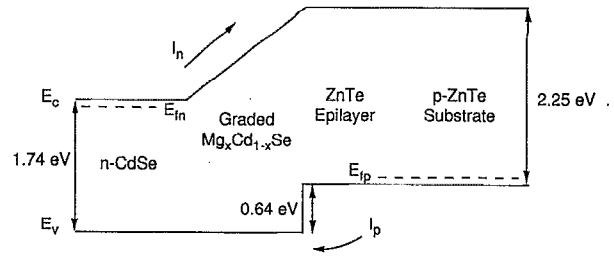

FIG. 3. Schematic diagram showing the CBE and VBE for the graded injector device at flatband. The graded $Mg_xCd_{1-x}Se$ region facilitates electron injection into the higher band-gap material.

which is adapted from Ref. 21 and hence is called a McCaldin diagram. This figure shows the common wide band-gap binary II-VI compounds, along with other common semiconductors for comparison purposes. The band offsets in this diagram are those predicted by Harrison's linear combination of atomic orbitals (LCAO) method.[22]

Examining Fig. 1, we note first that none of the wide band-gap II-VI compounds can be conventionally doped both *n* and *p* type, and only one, ZnTe, can be conventionally doped *p* type. Thus, it is logical that a wide band-gap LED design should incorporate ZnTe. Also, since interface states caused by dislocations can have severely detrimental effects on the electrical and optical properties of a device, it is highly desirable to have a device design that uses only nearly lattice-matched II-VI compounds. From Fig. 1, we see that CdSe can be doped *n* type and has only a 0.4% lattice mismatch to ZnTe. Thus, an *n*-CdSe/*p*-ZnTe heterojunction shows some promising characteristics for a wide band-gap LED. No other combination of II-VI compounds allows for both a small lattice mismatch and formation of a conventionally doped *pn* heterojunction. However, the experimental VBO between CdSe and ZnTe is 0.64 ± 0.07 eV,[23] with the ZnTe VBE higher than the CdSe VBE. Since the CdSe band gap is 1.74 eV, this gives a CBO of roughly 1.15 eV, resulting in a type II heterojunction which favors carrier injection into the smaller band-gap CdSe layer.[24] The simulations in the following section confirm that a simple *n*-CdSe/*p*-ZnTe heterojunction device suffers from interface recombination and hole injection.

To try to improve on the simple CdSe/ZnTe device, we look first at another McCaldin diagram shown in Fig. 2. In addition to the familiar binary II-VI compounds, this figure also shows magnesium based II-VI compounds, specifically MgS, MgSe, and MgTe. $Mg_xCd_{1-x}Se$ and $Mg_xZn_{1-x}Te$ ternaries are represented by the shaded regions on this diagram. Again, the LCAO method is used to determine the VBO. The room temperature band gap of MgTe is 3.57 eV.[25] The band gap of MgSe is uncertain, with reported values ranging from 3.6 eV at 77 K (Ref. 26) to 5.63 eV at 90 K.[27] The first value gives a room-temperature band gap of roughly 3.5 eV. This is smaller than the MgTe band gap, which is unusual since typically, if two semiconductors have a common cation, then the semiconductor with the smaller anion will have the larger band gap. Thus, we suspect that the MgSe band gap should be greater than 3.5 eV, which would be advantageous to our device performance. In our simulations, however, we use the less favorable of the two quoted values for the band gap of MgSe.

The predicted MgSe to CdSe VBO is such that a $Mg_xCd_{1-x}Se$ ternary of the proper composition can have a zero CBO to ZnTe while maintaining a similar VBO as in a CdSe/ZnTe heterojunction. From Fig. 3, we see that by grading from CdSe to $Mg_xCd_{1-x}Se$, we should be able to form a graded region that will facilitate electron injection into the ZnTe layer, while the VBO between $Mg_xCd_{1-x}Se$ and ZnTe will continue to block hole injection. This will hold as long as the VBE of $Mg_xCd_{1-x}Se$ is not more than a few tenths of an electron volt above the VBE of CdSe. Thus, the operation of this device is not very sensitive to the validity of the LCAO method or the common anion rule. This graded injector concept for wide band-gap light emission was first proposed in Ref. 4. Details of the operation of this device and simulation results will be given in the following section.

Figure 2 shows that a $Mg_xZn_{1-x}Te$ ternary has a large CBO and a small VBO to ZnTe. This allows us to use $Mg_xZn_{1-x}Te$ layers to confine electrons without affecting hole transport. Also, by forcing the bulk recombination to occur in a $Mg_xZn_{1-x}Te$ layer, we can extend the wavelength of light emitted from our device into the blue. The following section will examine in more detail the use of $Mg_xZn_{1-x}Te$ layers in wide band-gap LEDs.

IV. RESULTS AND DISCUSSION

A. CdSe/ZnTe

As discussed in Sec. II, an *n*-CdSe/*p*-ZnTe heterojunction has favorable lattice match and dopability characteristics for a wide band-gap LED; however, the band alignments in this heterojunction favor interfacial recombination over thermionic injection. In this section we will examine results from numerical simulations of an *n*-CdSe/*p*-ZnTe heterojunction, in order to determine the feasibility of such a device. All of the simulations presented below are done at room temperature. We assume a donor

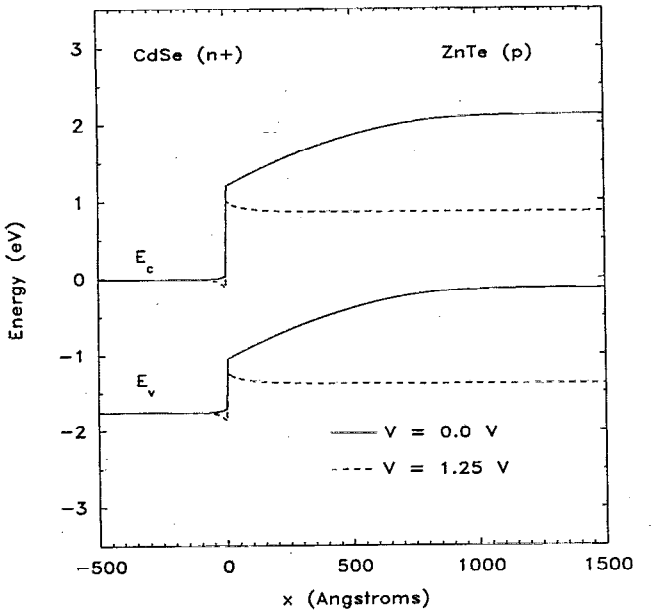

FIG. 4. CBE and VBE for an *n*-CdSe/*p*-ZnTe heterostructure at 0.0 and 1.25 V forward bias. Zero on the horizontal axis corresponds to the CdSe/ZnTe interface.

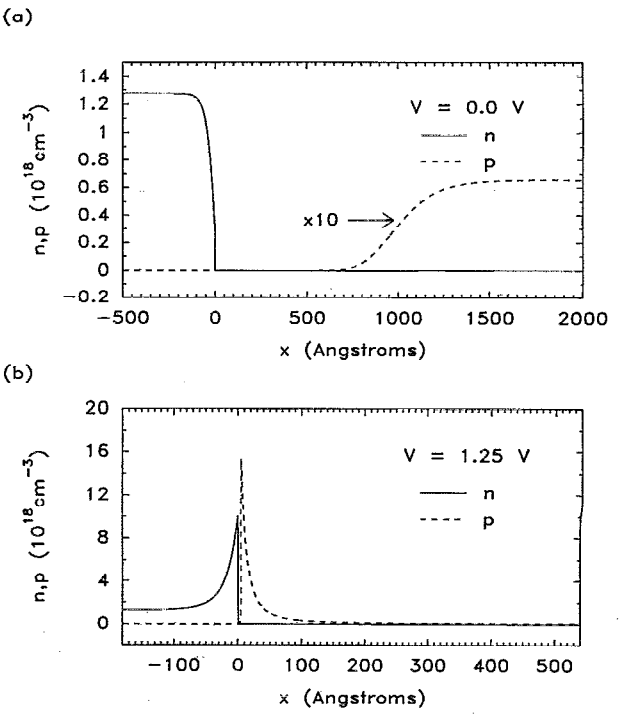

FIG. 5. (a) Electron and hole charge densities for an *n*-CdSe/*p*-ZnTe heterostructure at 0.0 V forward bias. (b) At 1.25 V forward bias, high carrier concentrations occur at the heterojunction interface.

concentration of 1×10^{19} for *n*-CdSe and an acceptor concentration of 1×10^{17} cm^{-3} for *p*-ZnTe. Ionized donor and acceptor concentrations are given by Eqs. (6) and (7). For the interfacial traps we assume a density of 1×10^{11} cm^{-2} and cross sections of 1×10^{-14} cm^{2}.

Figure 4 shows the CBE and VBE of a CdSe/ZnTe heterojunction at forward biases of 0.0 and 1.25 V. Figure 5 shows the electron and hole concentrations at these same biases. At zero bias, we note that both the CdSe and the ZnTe are depleted at the interface. As we apply a forward bias, the depletion width decreases, and at a large enough bias, electrons and holes begin to accumulate at the interface. Figure 6 shows the electron current densities at 0.75 and 1.25 V forward biases. Referring to Eqs. (15) and (16) we note that the slope of a current density plot at a given point gives a direct measure of the rate of recombination at that point. At a bias of 0.75 V, we see that all of the recombination occurs at the CdSe/ZnTe interface. At a higher bias of 1.25 V, all of the bulk recombination occurs in the CdSe region, indicating that holes are being injected into the CdSe layer rather than electrons into the wider band-gap ZnTe region. Thus, numerical simulations of an *n*-CdSe/*p*-ZnTe heterojunction explicitly demonstrate that this design will not produce efficient light emission in the wide band-gap ZnTe material. Instead, recombination in the CdSe and at the CdSe/ZnTe interface will dominate.

B. CdSe/$Mg_xCd_{1-x}Se$/ZnTe graded device

The next design that we present offers an improvement on the CdSe/ZnTe design. By including a graded $Mg_xCd_{1-x}Se$ region between the CdSe and ZnTe layers, we hope to facilitate electron injection, while continuing to block hole injection into the CdSe layer. The material parameters for the CdSe layer are the same as in the previous device. Two types of ZnTe are used in this simulation: an undoped ZnTe epilayer, and a lightly (1×10^{17} cm^{-3}) doped *p*-ZnTe substrate with an oxygen center 0.4 eV below the CBE.[28,29] The oxygen center is needed to accurately model the substrates used in actual devices.

The $Mg_xCd_{1-x}Se$ layer is graded from zero Mg concentration to a concentration such that there is no CBO to ZnTe (see Fig. 3). The VBO between MgSe and CdSe has not yet been measured experimentally; however, Harrison's LCAO method predicts a small VBO between the two materials. Since small changes in the CdSe/MgSe VBO do not significantly affect the operation of this device, we use the common anion rule in our calculations in the absence of experimental band offsets. For a MgSe band gap of 3.5 eV, this gives a value of 0.66 for x at the $Mg_xCd_{1-x}Se$/ZnTe interface. The doping of the graded $Mg_xCd_{1-x}Se$ region is *n* type at the CdSe interface and undoped at the ZnTe interface. These doping parameters account for the likelihood that $Mg_xCd_{1-x}Se$ will not be dopable *n* type for high Mg concentrations. The thickness of the graded region was chosen to be 200 Å. A thinner graded region decreases the accumulation of electrons near the CdSe/$Mg_xCd_{1-x}Se$ interface, making electron injection more difficult, while increasing the thickness might prevent the graded $Mg_xCd_{1-x}Se$ from being coherently strained to the ZnTe.

Figure 7 shows the CBE and VBE for this device at 0.0 and 2.0 V forward bias. Figure 8 gives the hole and electron charge densities at the same biases. At zero bias the

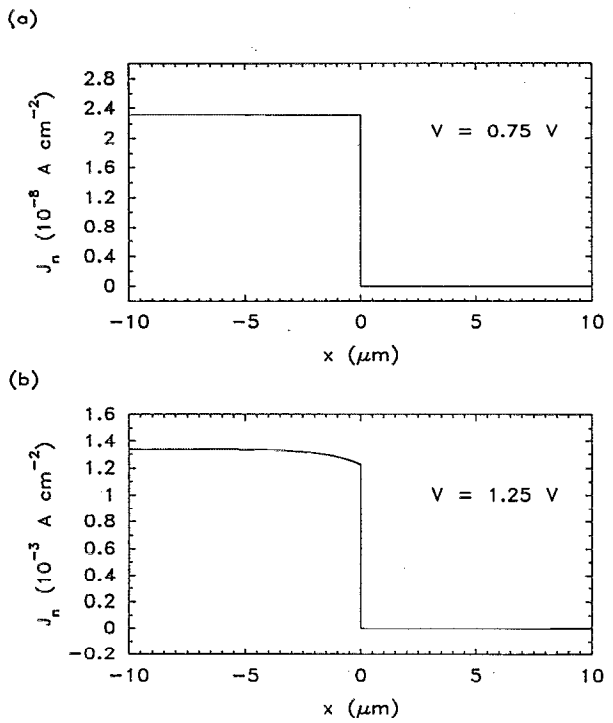

FIG. 6. Electron current densities for an n-CdSe/p-ZnTe heterostructure at (a) 0.75 V applied bias and (b) 1.25 V applied bias. Since the recombination rate is proportional to the slope of the current density, this figure shows that interfacial recombination dominates the device operation at lower applied biases, and that holes are injected into the CdSe at higher applied biases.

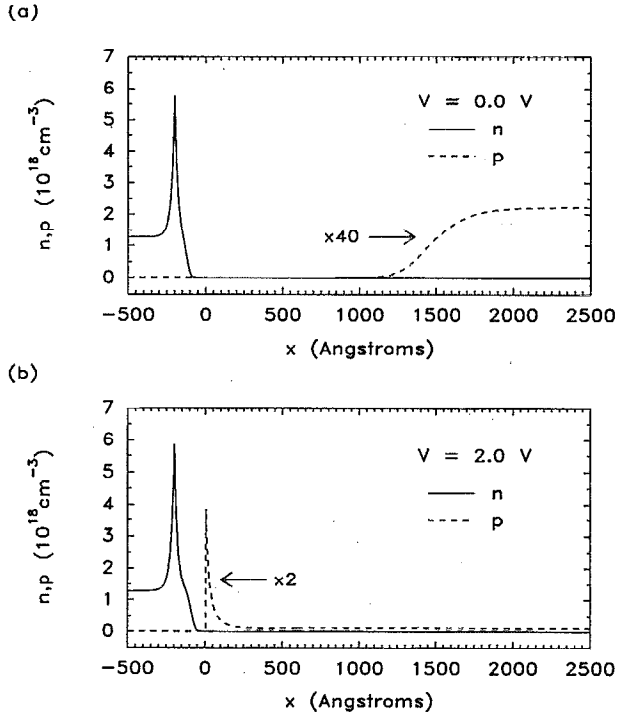

FIG. 8. Electron and hole charge densities for the graded injector device at (a) 0.0 V forward bias and (b) 2.0 V forward bias. Notice the spatial separation of accumulated charge.

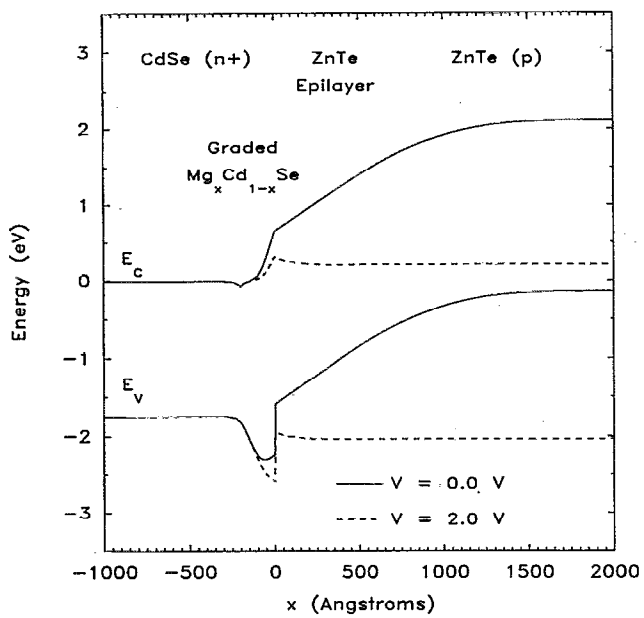

FIG. 7. CBE and VBE for the graded injector device at 0.0 and 2.0 V forward bias. In this figure and in all succeeding figures, zero on the horizontal axis corresponds to the right-hand side of the graded $Mg_xCd_{1-x}Se$ layer.

ZnTe layer is depleted at its interface with the graded $Mg_xCd_{1-x}Se$ region, while electron accumulation occurs at the interface between the CdSe and the graded $Mg_xCd_{1-x}Se$ region. As a forward bias is applied to the device, the depletion width in the ZnTe layer decreases and eventually holes accumulate at the $Mg_xCd_{1-x}Se$/ZnTe interface. An important point to note here is that whereas in the CdSe/ZnTe device, electron and hole accumulation at the heterojunction interface led to high rates of nonradiative recombination, in the graded device, electron and hole accumulations are spatially separated. This leads to a considerable reduction in the amount of nonradiative recombination that occurs at the interfaces. As we continue to increase the forward bias, Fig. 9 shows that electron injection occurs prior to any significant hole injection. Recall that the slope in the current density is a measure of the recombination rate, so the slope in j_n on the right-hand side of Fig. 9 shows that injected electrons are recombining in the ZnTe material. Since the total current is constant throughout the device, the slope in j_p is simply the negative of the slope of j_n. Notice that interfacial recombination dominates the operation of the device only at lower voltages, and that bulk recombination begins to dominate at higher voltages.

The graded $Mg_xCd_{1-x}Se$ layer facilitates electron injection as follows. At zero bias, the barrier to electron injection is essentially the same in the graded device as it is in the CdSe/ZnTe device. As we forward bias the CdSe/ZnTe device, the barrier to electron injection remains essentially constant, determined by the fixed CBO between

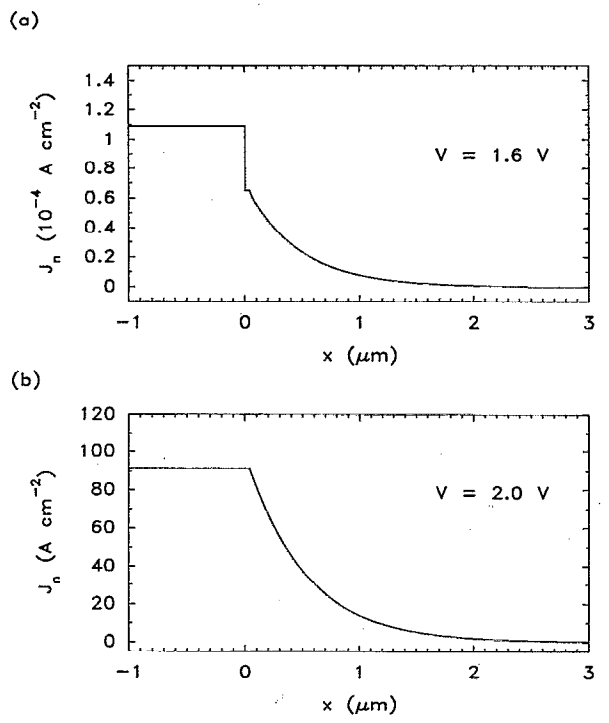

FIG. 9. Electron current density for the graded injector device at (a) 1.6 V forward bias and (b) 2.0 V forward bias. The second flat portion in (a) corresponds to the ZnTe epilayer.

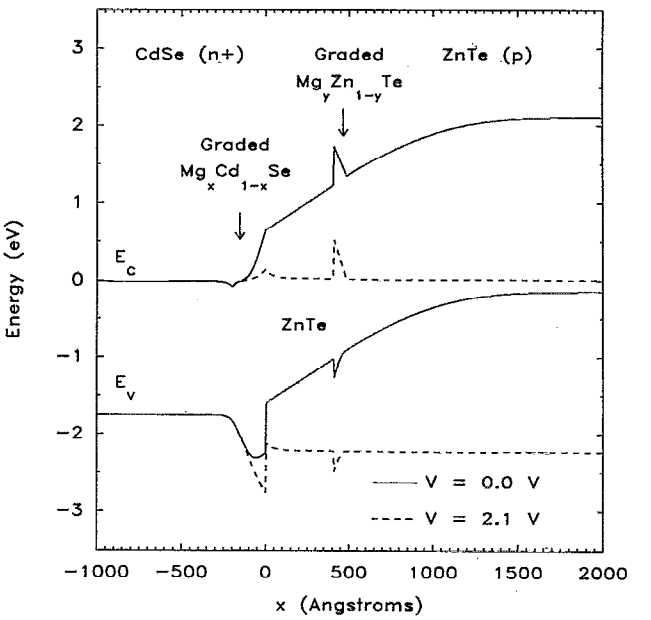

FIG. 10. CBE and VBE for the graded injector device with an electron confining layer at 0.0 and 2.0 V forward biases. Note the undesirable deviation from the common anion rule used for the $Mg_yZn_{1-y}Te$ to ZnTe band offset.

the two materials. In the graded device however, as we apply a forward bias, more and more electrons accumulate within the graded $Mg_xCd_{1-x}Se$ layer. This accumulation of electrons causes the bands to bend downwards, as seen in Fig. 7, thereby reducing the barrier to electron injection.

Figure 9 shows the electron and hole current densities at 1.6 and 2.0 V forward bias. Very few of the injected electrons actually recombine in the ZnTe epilayer, since the diffusion length in ZnTe epilayers is much greater than the the thicknesses of the epilayers used in our devices. Most of the electrons recombine in the ZnTe substrate, which results in red light emission because of the oxygen center. Thus, for the purposes of high efficiency green light emission, and for laser applications, we need to be able to confine injected electrons to the ZnTe epilayer. The next design that we propose offers a method of implementing this.

C. Graded device with confining layer

To confine injected electrons to the ZnTe epilayer, we refer again to Fig. 2. This figure shows that a $Mg_xZn_{1-x}Te$ ternary will have a larger band gap than ZnTe with most of the difference going into the conduction band. We propose to insert a $Mg_yZn_{1-y}Te$ confining layer between the ZnTe epilayer and the ZnTe substrate. Again, the VBO between MgTe and ZnTe has yet to be experimentally determined; however, the LCAO method predicts a small VBO which is desirable for our device operation. In our calculations, we assume a less favorable case with two thirds of the band offset going into the conduction band and one third in the valence band. We do this to demonstrate that the performance of our devices is not highly dependent on the validity of the common anion rule. Using the MgTe band gap of 3.57 eV and choosing a conduction-band barrier height of 0.5 eV gives a value of 0.57 for y at the $Mg_yZn_{1-y}Te$ to ZnTe epilayer interface. The $Mg_yZn_{1-y}Te$ confining layer is graded to avoid blocking holes from entering the ZnTe epilayer. If a more favorable VBO is used, then the $Mg_yZn_{1-y}Te$ confining layer need not be graded and also the Mg concentration will be less for the same barrier height, resulting in less strain. The width of the graded $Mg_xZn_{1-x}Te$ region only needs to be thick enough to prevent electrons from tunneling through to the ZnTe substrate. We use 75 Å in our calculations.

Figure 10 shows the CBE and VBE for this device at forward biases of 0.0 and 2.0 V. Figure 11 gives the hole and electron charge densities at these same biases. Until the onset of electron injection, this device behaves in much the same way as the previous device. After the onset of electron injection, however, we see that the confining layer prevents electrons from entering the ZnTe substrate. In Fig. 12, the electron current densities for this device at a forward bias of 2.0 V show that, with the addition of the electron confining layer, the bulk recombination in the device is confined to the ZnTe epilayer. It will also be noticed that interfacial recombination comprises a significant portion of the total recombination in the device. Interfacial recombination plays a larger role at small biases, and becomes less significant as the bias is increased. Quantitative calculations of radiative recombination rates and quantum efficiencies will depend largely on the specific properties of the interfaces in each device.

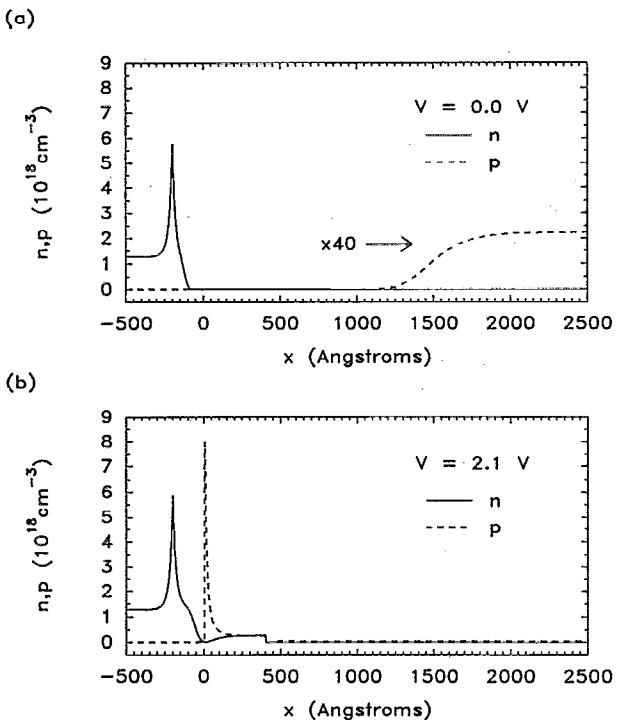

FIG. 11. Electron and hole charge densities for the graded injector device with a confining layer at (a) 0.0 V forward bias and (b) 2.1 V forward bias.

D. Tunable band-gap LED

We lastly consider a device design that will allow the wavelength of light emitted from the device to be tuned continuously from the green to the blue wavelength regimes. This design was first proposed in Ref. 4. The basic idea behind the device is to have the radiative recombination occur in a $Mg_yZn_{1-y}Te$ layer, where y can be adjusted to obtain the desired band-to-band recombination energy. Figure 13 shows a schematic of the proposed device at flatband. Note that we have used the common anion rule in simulating this device, so there is no VBO between ZnTe and MgZnTe ternaries. This allows us to forego the grading of the $Mg_zZn_{1-z}Te$ confining layer that was needed in the previous device. Note that we do this for convenience and clarity of presentation only; the device concept does

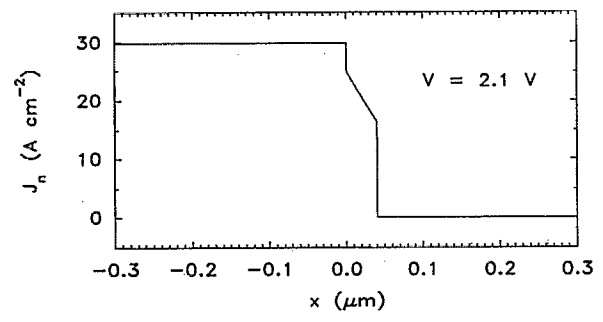

FIG. 12. Electron current densities for the graded injector device with a confining layer at a forward bias of 2.1 V. The two regions showing a very large slope in the current density plot correspond to the $Mg_xCd_{1-x}Se$/ZnTe and ZnTe/$Mg_yZn_{1-y}Te$ interfaces, respectively.

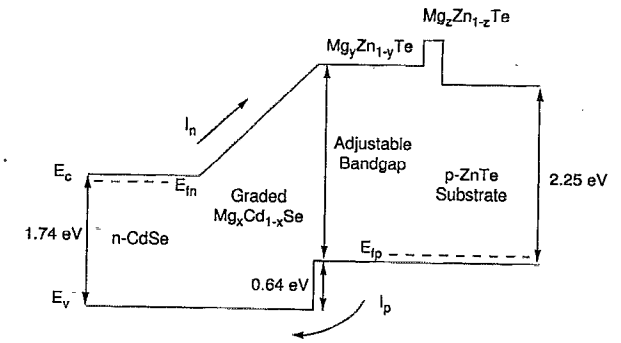

FIG. 13. Schematic diagram showing the CBE and VBE for the tunable band-gap LED at flatband.

not depend on the validity of the common anion rule. Figure 14 shows the CBE and VBE of the device at 0.0 and 2.25 V forward bias. Figure 15 shows the hole and electron charge densities at these same biases. From these figures we see again that the graded $Mg_xCd_{1-x}Se$ layer enhances electron injection into the wider band-gap material, while spatially separating interfacial charge accumulations. Figure 16 shows the electron current densities for this device at a forward bias of 2.25 V. In this figure we see that all of the bulk recombination occurs in the $Mg_yZn_{1-y}Te$ epilayer. Thus, the wavelength of light emitted from this device can be varied from green to well into the blue wavelength regime, depending on the the Mg concentration used in the $Mg_yZn_{1-y}Te$ epilayer. The tunable band-gap LED operates in much the same manner as the previous device presented above, with the exception that the wavelength of light emission is tunable from green to blue.

V. CONCLUSION

We present the numerical simulation and design of novel wide band-gap II-VI LEDs. The drift-diffusion

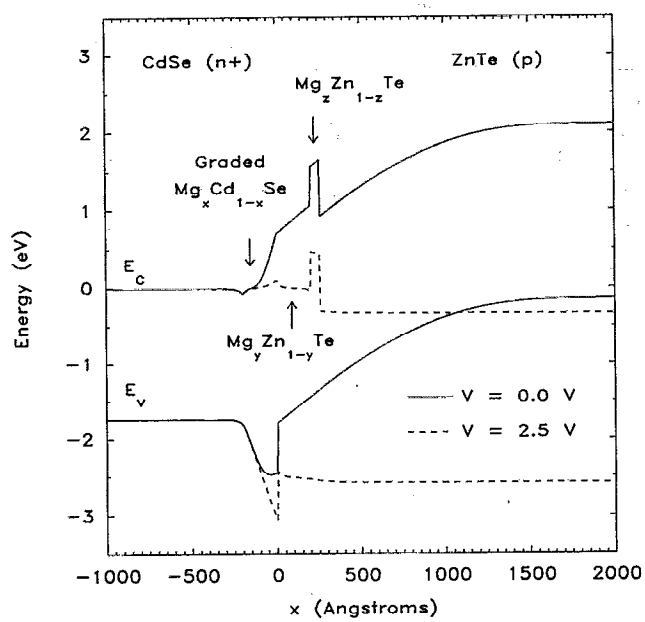

FIG. 14. CBE and VBE for the tunable band-gap LED at 0.0 and 2.5 V forward bias.

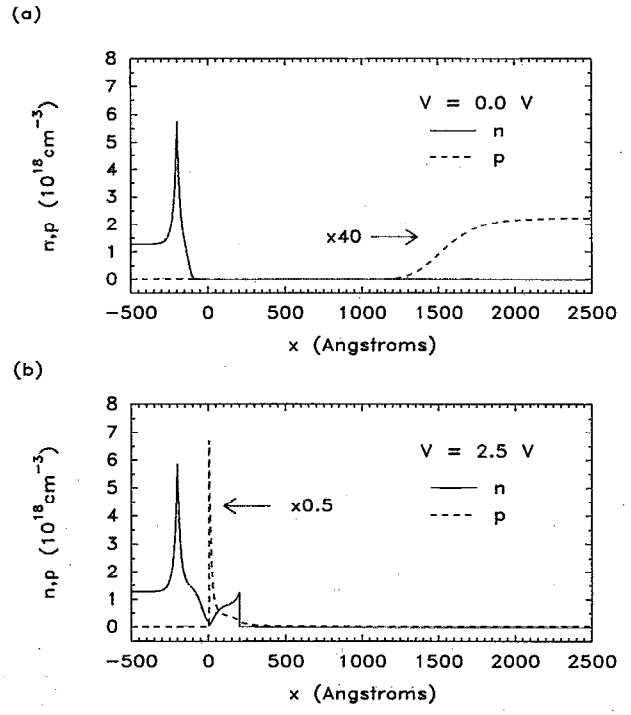

FIG. 15. Electron and hole charge densities for the tunable band-gap LED at (a) 0.0 V forward bias and (b) 2.5 V forward bias. Notice the accumulation of both holes and electrons in the $Mg_yZn_{1-y}Te$ layer at 2.5 V bias.

model, modified to account for heterojunctions, is used in the simulations. All of the designs we present incorporate both *n*-CdSe and *p*-ZnTe. ZnTe is used because it is the only wide band-gap II-VI compound that can be conventionally doped *p* type. CdSe, with its small lattice mismatch to ZnTe and its *n*-type dopability is then the logical compound to use for the formation of a II-VI *pn* heterojunction with ZnTe. A simple *n*-CdSe/*p*-ZnTe heterostructure is first analyzed. Simulation results for this design show high interface recombination rates and hole injection into the smaller band-gap CdSe layer. The CdSe/$Mg_xCd_{1-x}Se$/ZnTe device proposed by Phillips *et al.*, improves on the CdSe/ZnTe heterojunction design by incorporating a graded $Mg_xCd_{1-x}Se$ electron injector. The addition of this layer significantly reduces interface recombination and facilitates electron injection into the wide band-gap ZnTe layer. A further improvement on this design utilizes a $Mg_xZn_{1-x}Te$ confining layer which restricts bulk recombination to the ZnTe epilayer. Finally, we present a tunable band-gap LED, in which the bulk recombination occurs in a $Mg_xZn_{1-x}Te$ epilayer. The Mg concentration then determines the wavelength of the light emitted from the device, which can be varied from green to well into the blue wavelength regime.

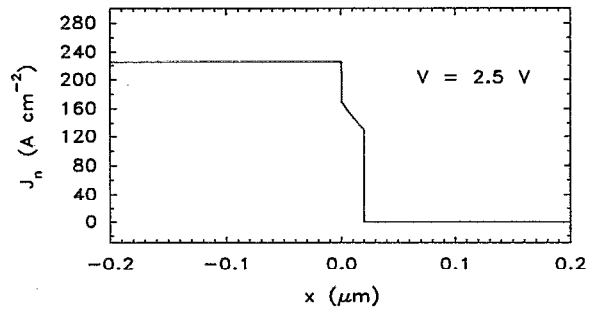

FIG. 16. Electron current density for the tunable band-gap LED at 2.5 V forward bias.

ACKNOWLEDGMENTS

The author wishes to thank Y. X. Liu, R. R. Marquardt, and D. Z.-Y. Ting for many useful discussions. One of us (E.T. Yu) would like to acknowledge financial support from the AT&T Foundation. This work was supported by the Office of Naval Research under Grant No. N00014-90-J-1742.

[1] J. Qiu, J. M. DePuydt, H. Cheng, and M. A. Haase, Appl. Phys. Lett. **59**, 2992 (1991).
[2] M. A. Haase, J. Qiu, J. M. DePuydt, and H. Cheng, Appl. Phys. Lett. **59**, 1272 (1991).
[3] J. O. McCaldin, T. C. McGill, and C. A. Mead, Phys. Rev. Lett. **36**, 56 (1976).
[4] M. C. Phillips, M. W. Wang, J. F. Swenberg, J. O. McCaldin, and T. C. McGill (unpublished).
[5] W. van Roosbroeck and W. Shockley, Phys. Rev. **94**, 1558 (1954).
[6] R. N. Hall, Proc. Inst. Electr. Eng. Part B **106**, Suppl. No. 17, 923 (1960).
[7] W. Shockley and W. T. Read, Phys. Rev. **87**, 835 (1952).
[8] A. H. Marshak, IEEE Trans. Electron Devices **36**, 1764 (1989).
[9] J. E. Sutherland and J. R. Hauser, IEEE Trans. Electron Devices **24**, 363 (1977).
[10] A. H. Marshak and K. M. van Vliet, Solid-State Electron. **21**, 419 (1978).
[11] M. S. Lundstrom, *Fundamentals of Carrier Transport* (Addison-Wesley, Reading, 1990).
[12] P. E. Dodd, T. B. Stellwag, M. R. Melloch, and M. S. Lundstrom, IEEE Trans. Electron Devices **38**, 1253 (1991).
[13] J. W. Harrison and J. R. Hauser, J. Appl. Phys. **47**, 292 (1976).
[14] A. G. Thompson and J. C. Woolley, Can. J. Phys. **45**, 255 (1967).
[15] M. Kurata and J. Yoshida, IEEE Trans. Electron Devices **31**, 467 (1984).
[16] H. C. Chan and T. J. Shieh, IEEE Trans. Electron Devices **38**, 2427 (1991).
[17] X. Aymerich-Humet, F. Serra-Mestres, and J. Millan, Solid-State Electron. **24**, 981 (1981).
[18] W. H. Press, B. P. Flannery, S. A. Teukolsky, and W. T. Vetterling, *Numerical Recipes* (Cambridge, New York, 1986).
[19] G. B. Tait, Solid-State Electron. **32**, 369 (1989).
[20] L. J. Turgeon and D. H. Navon, IEEE Trans. Electron Devices **25**, 837 (1978).
[21] J. O. McCaldin, J. Vac. Sci. Technol. A **8**, 1188 (1990).
[22] W. A. Harrison, J. Vac. Sci. Technol. **14**, 1016 (1977).
[23] E. T. Yu, M. C. Phillips, J. O. McCaldin, and T. C. McGill, J. Vac. Sci. Technol. B **9**, 2233 (1991).
[24] J. O. McCaldin, *Growth and Optical Properties of Wide-Gap II-VI Low-Dimensional Semiconductors*, edited by T. C. McGill, C. M. Sotomayor Torres, and W. B. Gebhardt (Plenum, New York, 1989), pp. 39–51.
[25] J. Marine, T. Ternisien D'ouville, B. Schaub, A. Laugier, D. Barbier, J. C. Guillaume, J. F. Rommeluere, and J. Chevallier, J. Electron. Mater. **7**, 17 (1978).
[26] H. Okuyama, K. Nakano, T. Miyajima, and K. Akimoto, Jpn. J. Appl. Phys. Part 2 Lett. **30**, L1620 (1991).
[27] H. Mittendorf, Z. Physik **183**, 113 (1965).
[28] J. L. Merz and R. T. Lynch, II-VI Semiconducting Compounds 1967 International Conference, 1967, p. 731.
[29] J. J. Hopfield, D. G. Thomas, and R. T. Lynch, Phys. Rev. Lett. **17**, 312 (1966).